AIAA Region III Student Conference
University of Kentucky-Paducah Student Chapter 4 - 5 April 2003

SENSITIVITY OF OPTIMAL CONFORMING AIRFOILS TO EXTERIOR SHAPE

Shawn E. Gano *
Department of Aerospace and Mechanical Engineering
University of Notre Dame
Notre Dame, Indiana
Email: sgano@nd.edu

Abstract

Interest in the design and development of unmanned aerial vehicles (UAVs) has increased dramatically in the last decade. This research is part of a development effort that involves the design of a buckle-wing UAV that "morphs" in a way which facilitates variations in wing loading, aspect ratio and wing section shapes. The buckle-wing consists of two highly elastic beam-like lifting surfaces joined at the outboard wing tips in either a pinned or clamped configuration. The Buckle-Wing UAV is capable of morphing between a separated wing configuration designed for maneuverability, to a single fixed wing configuration designed for long range/high endurance. This morphing concept leads to extra design challenges in the fact that one airfoil, which must have high range/endurance capabilities, must also separate in such a way that the two airfoils give good maneuverability characteristics. This problem is a multiobjective multilevel optimization process. Because the optimization is multilevel the gradients of the suboptimization are needed. Normally, these gradients are computed via finite differencing. However, this adds to the computational cost tremendously. This paper describes and applies a method to find post-optimal solution sensitivity to problem parameters or the gradients at a much lower cost. This method is found to save 75% of the computing time over using the finite differencing scheme when applied to this problem.

*Graduate Research Assistant, Student Member AIAA

Nomenclature

α	Angle of attack
Δ	Represents a perturbation in a variable
λ_i	The Lagrange multiplier of the ith constraint
c_d	Drag coefficient
c_l	Lift coefficient
c_p	Pressure coefficient
F	Objective Function
g_j	The jth constraint
$\mathbf{l}$	Lower bound
P_i	The ith problem paramter
^{T}	Transpose
$\mathbf{u}$	Upper bound
w_n	The nth design weight
$\mathbf{x}$	Design variable vector
x_i	The ith design variable
*	Optimum Quantity

1 Introduction

There has been a growing interest in the development of unmanned arial vehicles (UAVs) for a variety of missions. These include video and IR surveillance, communication relay links, and the detection of biological, chemical, or nuclear materials. These missions are ideally suited to UAVs that are either remotely piloted or autonomous.

Unmanned aerial vehicles (UAVs) are an ideal application area for morphing aircraft structures. Existing fixed

geometry UAV designs have generally been designed for maximum flight endurance and range to provide extended surveillance (i.e., single mission capability). Future classes of UAVs with morphing airframe geometries are envisioned for achieving both endurance and maneuverability in a single vehicle (i.e., multiple mission profiles).

A typical mission that a multi-role UAV could perform is depicted in Figure 1. This mission would include takeoff, cruise to some desired location as efficiently as possible, then it would encounter a flight situation in which high maneuverability is essential, then an efficient cruise back, and finally landing. In takeoff, high-g maneuvers, and landing, high lift is desired with much less emphasis on the level of drag. When cruising, however, maximum range/endurance is desired so the lift to drag ratio is important.

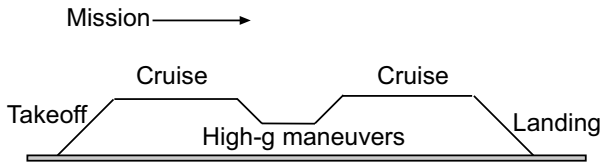

Figure 1. Typical mission scenario.

An adaptive airframe UAV concept that could accommodate such a versatile mission is a unique morphing UAV referred to as the Buckle-Wing, that is being developed at the University of Notre Dame. The wing consists of two highly elastic beam-like lifting surfaces joined at the outboard wing tips in either a pinned or clamped configuration. The UAV is capable of morphing between a separated wing configuration designed for maneuverability to a single fixed wing configuration designed for long range and/or high endurance.

The Buckle-Wing design has many advantages over a traditional UAV design because the trade off for maneuverability and range/endurance can be somewhat decoupled. Allowing the performance of each category to be greater than if a single design had them as competing objectives. With this new capability comes new design challenges.

The focus of the paper by Gano et. al.[6] was to formulate and solve the problem of finding the optimal shapes for the airfoils such that the combined buckled and conformed system are optimal. However, the problem was a multilevel optimization problem that was very computationally expensive. Furthermore, the objective function of the system optimization depended on the value from a sub optimization problem. This added tremendously to the computational cost because the upper level optimization implored the efficient sequential quadratic programming algorithm which requires gradients of the objective function and constraints. Gradients of the optimization were not available so finite differencing was required. In this paper the use of sensitivity analysis based on the first order Kuhn-Tucker optimality conditions for a more efficient means of calculating the lower level optimization gradients with respect to the upper level optimization variables is given and tested.

In the following sections the Buckle-Wing UAV is described in greater detail, then a description of the Buckle-Wing and conforming airfoil problems and solutions are given. Followed next by a description of the sensitivity analysis for the lower level optimization problem. Two academic problems and the conforming airfoil problem, the lower level optimization problem, are then tested using this method and the results compared to finite differencing.

2 Buckle-Wing UAV Description

The morphing-wing UAV concept that is being developed is the unique Buckle-Wing biplane illustrated in Figures 2 and 3. This aircraft will be capable of independently changing wing loading, aspect ratio, and wing section shape while in flight.

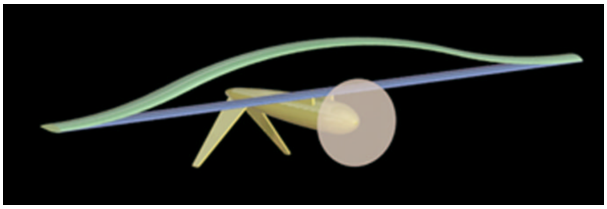

Figure 2. Buckle-Wing in bi-plane configuration.

The Buckle-Wing consists of a lower lifting surface that is relatively stiff and an upper lifting surface with outboard attachments to the lower wing and the capability of large, elastic-buckling deformations in pinned, clamped or various constrained sliding configurations. A variety of morphing deformations can be induced through controlled buckling of the elastic lift surfaces.

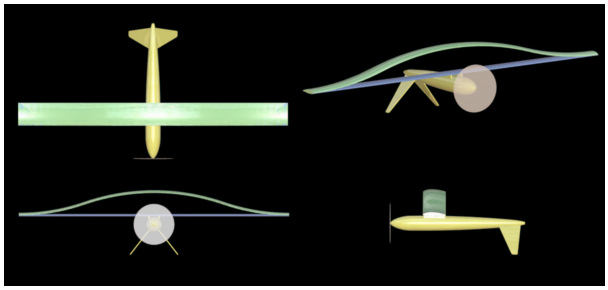

Figure 3. Buckle-Wing from different perspectives in bi-plane configuration.

The buckle-wing acts as a fused single wing in the absence of applied buckling loads and morphs into vertically stacked wings when separated via application of controlled buckling loads. A variety of actuators exist for supplying/controlling the buckling loads[5]. Outboard actuators can apply axial loads and a central actuator can apply a transverse load to separate the two lifting surfaces via buckling deformation, thereby providing the biplane characteristics and decreased wing loading. Actuators in the wing-rib-structure can be used to attain smaller-scale deformations of the airfoil. The two wing surfaces will join to form a single wing with a much higher aspect ratio and increased wing loading in the absence of actuation forces.

3 Buckle-Wing and Conforming Airfoil Problem

The multiobjective optimization seeks to find an exterior airfoil that maximizes high range and/or endurance performance, that can be decomposed into two airfoils, that when separated produce maximum high lift performance for maneuverability. This is posed as a multiobjective and multilevel optimization problem for determining the buckle-wing UAVs conforming airfoils.

A flowchart of the optimization problem is shown in Figure 4. The system level optimizer varies the geometry of the fused airfoil (external geometry) and the angle of attack for the fused deployment to achieve the highest endurance (c_l/c_d maximum) for the fused shape, and the most maneuverable (c_l maximum) separated configuration. For each iteration the performance of the fused airfoil is computed and then the geometry is input to a sublevel optimization problem that finds the optimal separated airfoil geometries for maneuverability. The sublevel optimization is solved for the current exterior airfoil iterate. In this sub optimization problem the angle of attack of the UAV, when in the separated configuration, is also determined. The optimal value of c_{lmax} is found and then passed back to the system level. This is a multiobjective, multilevel optimization formulation.

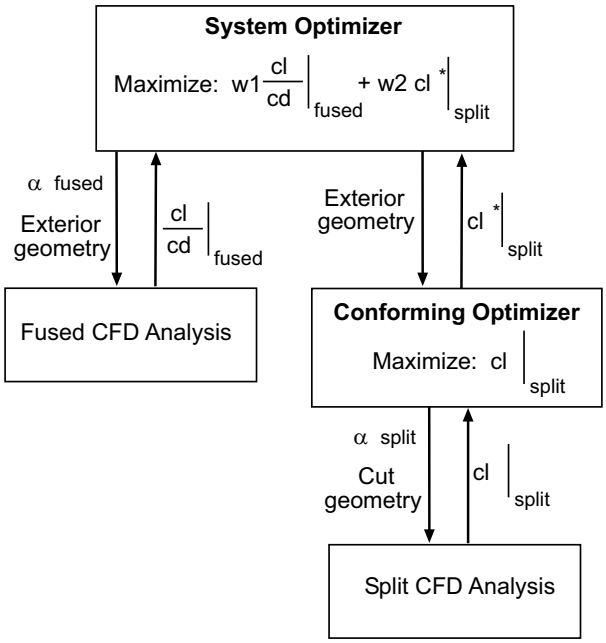

Figure 4. Flowchart for the conforming airfoil optimization framework.

The flowchart in Figure 4 doesn't show the constraints that are imposed on the system. For the system level optimization there is a constraint on the lift coefficient that must minimally be produced by the fused airfoil, along with other possible aerodynamic constraints that may be desired. Structural constraints must also be enforced so that the airfoils don't become too thin. In the suboptimization problem, there are again general aerodynamic constraints and structural constraints. A minimal lift to drag ratio can also be used as a constraint.

The two airfoil configurations do compete because their geometries must conform with one another. Weights, w_1 and w_2, are added to the objective function so that the designer can control the importance of each objective.

The mathematical optimization statement can be posed as,

$$\begin{aligned} \text{maximize}: \quad & w_1 \left.\frac{c_l}{c_d}\right|_{fused} + w_2 \left. c_l^* \right|_{split} \\ \mathbf{x} & \\ \text{subject to}: \quad & \mathbf{l} \leq \begin{pmatrix} \left. c_l \right|_{fused} \\ \mathbf{Aero}(\mathbf{x}) \\ \mathbf{Struct}(\mathbf{x}) \\ \mathbf{x} \end{pmatrix} \leq \mathbf{u}. \end{aligned}$$

Where $\left. c_l^* \right|_{split}$ is the optimal value of the sub optimization airfoil conforming problem,

$$\begin{aligned} \text{maximize}: \quad & \left. c_l \right|_{split} \\ \mathbf{x}_{sub} & \\ \text{subject to}: \quad & \mathbf{l} \leq \begin{pmatrix} \left.\frac{c_l}{c_d}\right|_{split} \\ \mathbf{Aero}(\mathbf{x}_{sub}) \\ \mathbf{Struct}(\mathbf{x}_{sub}) \\ \mathbf{x} \end{pmatrix} \leq \mathbf{u}. \end{aligned}$$

The design variables for the main optimization consist of a parametrization of the fused geometry and its angle of attack. Further design variables are introduced in the sub problem and they consist of the airfoil parting geometry and the angle of attack for the craft in the buckled configuration.

The sub optimization problem was used instead of letting the system level optimizer handle all of the design variables because this insured a continuous design space. If the system level optimizer could change the cut and the fused shapes, then it would be possible that the shape of the cut would in fact not fit within the shape of the fused airfoil. If this occurred then there would be no way to perform the CFD analysis because the geometry would be not possible. It would be possible to set constraints on these shapes but this would be difficult to do using the methods of parametrization used (basis functions) to express the shape of the fused airfoil. If splines were used for describing both geometries then this problem could be written with a single level optimization, however there would need to be many control points on the surface and thus many design variables and therefore making the problem quite computationally expensive. Other methods are possible to rewrite this problem as a single level optimization but make the design space very complex. So at this stage in the research it has been decided to keep the coupling of the two optimizations separate.

The methods used to parameterize the geometry of both the fused shape and the cut play a large role in the computational expense of this optimization and is discussed in the next subsection. This is followed by the results obtained from the conforming airfoil problem.

3.1 Geometric Parametrization

The way in which the geometry of the fused airfoil and the cut are parameterized is important because it effects the number of design variables in the system and the shape possibilities. As the number of design variables increases the optimization algorithm needs more data especially in the form of gradients for each variable. Because CFD is very expensive this information is quite time consuming to calculate. On the other hand the more values used to describe the shape of these two geometries the greater the freedom the optimizer has to find the best possible shape. Two different methods have been used to describe the geometries. For the fused airfoil, basis functions were used and for the cut, cubic splines were used.

An approach used by Vanderplaats[23], called basis functions, was used to describe the fused airfoil shape. The method uses a set of airfoil geometries as a basis for creating new geometries. Design variables are used for the various weights of each of the basis shapes. Each of these weights are multiplied by their respective airfoil and then these shapes are summed up to form a new shape. Because all of the airfoils are smooth the resultant shape is guaranteed to be smooth and to have the appropriate characteristics, such as a rounded leading edge and a sharp trailing edge. This approach is preferred over using spline control points because it requires less design variables to make new airfoil shapes. However splines do have the capability of making any possible shape where the basis functions may not.

The cut shape could be described in terms of basis shapes as well. One approach would be to use a set of upper surfaces and lower surfaces as the basis. However in the test case presented in this paper spline control points are used to vary the shape of the cut. This was done in order to see what general shapes would be found for the cut and not to bias it with a small set of possible basis shapes.

3.2 Conforming Airfoil Results

In the paper by Gano et. al.[6] the conforming airfoil problem or the sub-optimization problem was solved. This is the problem that deal with finding the best cut through a given exterior airfoil shape to create two airfoils that when they were separated produced the most lift. The main results are shown graphically in Figure 5. In the top of the figure the fused airfoil is shown with a cut that was parameterized by 3 control points and 3

fixed nodes all fitted with a cubic spline curve. The three fixed nodes included one at the leading edge, one at the trailing edge and one near the trailing edge to insure that each split airfoil had a sharp trailing edge. In the center of Figure 5 the general shape of the split airfoils are given for the starting point and optimized shape is shown in the bottom of the Figure. Notice that the optimal cut makes a thin of a slice along the upper surface as was allowed by the variable bounds. The results in this paper agree well with the findings in that paper but address the issue on how to get the sensitivity of the lift produced by this system to the exterior airfoil that is sent down from the system level optimizer.

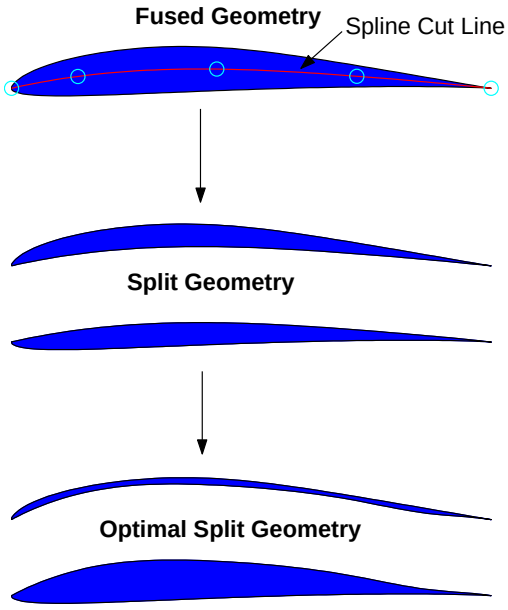

Figure 5. Conforming airfoil optimization geometries.

4 Post-Optimal Solution Sensitivity to Problem Parameters

The sensitivity of an optimum design to problem parameters was studied in the early 1980's. In work by Sobieszczanski-Sobieski et. al.[20] this sensitivity was derived exactly but was still expensive to compute. In later work by Barthelemy and Sobieszczanski-Sobieski[4] another method was derived to yield this sensitivity information with much less computational expense. This result is described briefly in this section.

Starting with the optimization problem,

$$\begin{aligned} &\text{maximize}: \quad F(\mathbf{x}, P_i) \\ &\quad \mathbf{x} \\ &\text{subject to}: \\ &\quad g_j(\mathbf{x}, P_i) \leq 0 \end{aligned}$$

where the vector $\mathbf{x}$ is the design variables, P_i are the problem parameters that are not changed by the optimization process, and g_j are the $j = 1 \ldots N$ constraints. Using the symbol * to denote quantities at the optimum,

$$F^* = F^*(\mathbf{x}^*(P_i), P_i) \tag{1}$$

$$g_j^* = g_j^*(\mathbf{x}^*(P_i), P_i) = 0. \tag{2}$$

Here we are only considering the constraints which are active. Using the chain rule we find the total sensitivity derivative of the optimum with respect to the problem parameters to be,

$$\frac{\mathrm{d}F^*}{\mathrm{d}P_i} = \frac{\partial F^*}{\partial P_i} + \left(\frac{\partial F^*}{\partial \mathbf{x}}\right)^T \frac{\partial \mathbf{x}^*}{\partial P_i} \tag{3}$$

Therefore once the optimum sensitivity derivatives of the design variables, $\frac{\partial \mathbf{x}^*}{\partial P_i}$, are computed Equation 3 yields the optimum sensitivity derivative of the objective function. However, these derivatives of the design variables are expensive to calculate so it is desirable to avoid computing them.

The Kuhn-Tucker conditions at the optimum point is defined as,

$$\frac{\partial F^*}{\partial \mathbf{x}} + \frac{\partial g_j^*}{\partial \mathbf{x}} \lambda_j^* = 0, \tag{4}$$

where $\frac{\partial g_j^*}{\partial \mathbf{x}}$ is the jacobian and λ^* is the vector of Lagrange multipliers. If the parameters P_i are perturbed then at the new optimal point the original active constraints remain active. Therefore,

$$\frac{\mathrm{d}g_j^*}{\mathrm{d}P_i} = \frac{\partial g_j^*}{\partial P_i} + \left(\frac{\partial g_j^*}{\partial \mathbf{x}}\right)^T \frac{\partial \mathbf{x}^*}{\partial P_i} = 0. \tag{5}$$

Multiplying Equation 4 by $\frac{\partial x^*}{\partial P_i}$ and substituting Equation 5 gives,

$$\left(\frac{\partial F^*}{\partial \mathbf{x}}\right)^T \frac{\partial \mathbf{x}^*}{\partial P_i} = (\lambda_j^*)^T \frac{\partial g_j^*}{\partial P_i}. \tag{6}$$

Substituting this into Equation 3 gives the final result,

$$\frac{\mathrm{d}F^*}{\mathrm{d}P_i} = \frac{\partial F^*}{\partial P_i} + (\lambda_j^*)^T \frac{\partial g_j^*}{\partial P_i}. \tag{7}$$

This equation is very efficient way to compute the sensitivity of the optimal objective function value with respect the the problem parameters. The Lagrange Multipliers are normally obtained through the optimization process, though if they are not can be easily computed. To compute Equation 7 one full optimization need to be computed then one function evaluation for each parameter. Compared to having to compute multiple full optimization runs this requires considerably less function evaluations. This result is put to use for three different problems in the next section.

5 Numerical Applications

A comparison of the sensitivity of the optimal solution to problem parameters found from finite differences and from the post-optimality method described in the previous section is given here for three different examples. The first two examples are simple cases and the third is the conforming airfoil problem.

5.1 Academic Example 1

The first problem used in comparing how the optimal solution varies when problem parameters are changed is,

$$\begin{aligned} \underset{\mathbf{x}}{\text{maximize :}} \quad & F = x_1 + x_2 \\ \text{subject to :} \quad & \\ & \frac{1}{x_1} + \frac{1}{x_2} + P \leq 0 \\ & x_1, x_2 > 0 \end{aligned}$$

Table 1. Academic Example 1: Finite Difference Results

P	F^*	x_1^*	x_2^*
-2.00	2.0000	1.0000	1.0000
-1.99	2.0101	1.0050	1.0050

Table 2. Academic Example 1: Post-Optimality Sensitivity Results

P	F^*	x_1^*	x_2^*	g	λ
-2.00	2.0000	1.0000	1.0000	0.00	1.0
-1.99	2.0000	1.0000	1.0000	0.01	-

Where P is the problem parameter, x_1 and x_2 are the design variables. In each case the starting design point was $x_1 = 2$ and $x_2 = \frac{2}{3}$. The parameter P was taken to be -2.

Using finite differencing, the problem was optimized for the original value of $P = -2$ and then re-optimized using a perturbed value of $P = -1.99$. The results from these two optimizations are listed in Table 1, where F^* is the optimal objective function value, x_1^* and x_2^* are the final design points.

From these results a forward finite difference yields a parameter sensitivity of,

$$\frac{\mathrm{d}F^*}{\mathrm{d}P} \approx \frac{F^*(P=-1.99) - F^*(P=-2)}{-1.99-(-2)} = 1.01 \tag{8}$$

Using the post-optimality sensitivity method the problem was optimized for the original value of the parameter as in the finite difference method. Then using the optimal design point found the objective function and the constraint were evaluated with a new parameter value of $P = -1.99$. No second optimization was preformed. The results obtained are presented in Table 2, where g is the value of the constraint and λ is the lagrange multiplier of the constraint.

From these results and using a forward difference to approximate the partial derivatives, the parameter sensitivity is,

$$\frac{\mathrm{d}F^*}{\mathrm{d}P} = \frac{\partial f}{\partial P} + \lambda \frac{\partial g}{\partial P}$$

$$\approx \frac{2-2}{-1.99-(-2)} + (1)\frac{0.01-0}{-1.99-(-2)} = 1. \qquad (9)$$

Because of the symmetry and size of this problem the parameter sensitivity can be found analytically to have a value of $\frac{\partial f^*}{\partial P} = 1$. So in this example the finite difference method was more expensive to compute and it gave results that were inferior to that of the post-optimality sensitivity method. This was also seen in studies by Sobieszczanski-Sobieski[21] et. al. in a similar study of a control-augmented structure problem. Also the sensitivity values of both methods converge to the same value as smaller step sizes of the parameter are used.

5.2 Academic Example 2

The second problem adds some complexity by including a direct influence of the parameter to the objective function. The problem is,

$$\begin{aligned} \underset{\mathbf{x}}{\text{maximize :}} \quad & F = x_1 - P x_2 \\ \text{subject to :} \quad & \\ & \frac{1}{x_1} + \frac{1}{x_2} + P \leq 0 \\ & x_1, x_2 > 0 \end{aligned}$$

Where P is the problem parameter, x_1 and x_2 are the design variables. In each case the starting design point was $x_1 = 2$ and $x_2 = \frac{2}{3}$. The parameter P was taken to be -2.

Using finite differencing, like in the first example, the problem was optimized for the original value of $P = -2$ and then re-optimized using a perturbed value of $P = -1.99$. The results from these two optimizations are listed in Table 3.

Table 3. Academic Example 2: Finite Difference Results

P	F^*	x_1^*	x_2^*
-2.00	2.9142	1.2071	0.8535
-1.99	2.9203	1.2114	0.8587

Table 4. Academic Example 2: Post-Optimality Sensitivity Results

P	F^*	x_1^*	x_2^*	g	λ
-2.00	2.9142	1.2071	0.8535	0.00	1.4566
-1.99	2.9057	1.2071	0.8535	0.01	-

From these values a forward finite difference yields a parameter sensitivity of,

$$\frac{\mathrm{d}F^*}{\mathrm{d}P} \approx 0.60614 \qquad (10)$$

Next the post-optimality sensitivity method was used. The problem was optimized for the original value of the parameter. Then using the optimal design point found the objective function and the constraint were evaluated with a new parameter value of $P = -1.99$. No second optimization was needed. The results obtained are presented in Table 4.

From these results the parameter sensitivity is found,

$$\frac{\mathrm{d}F^*}{\mathrm{d}P} \approx 0.60307 \qquad (11)$$

The two methods both predicted sensitivities that were very similar. Since these functions are easily evaluated, in the limit as the perturbation of the parameter decreased both methods predicted the same sensitivity.

The good agreement in results of both of these simple example problems show that the post-optimality sensitivity method, while requiring much less computational time, predicts the parameter sensitivity well. In the next example the much more expensive design problem, the conforming airfoil, is presented.

5.3 Conforming Airfoil Problem

Now the sub optimization or conforming airfoil problem is tested using again, both finite differencing and post optimality methods. The problem starts with a given exterior airfoil shape, which in the full buckle-wing problem would be governed by the system level optimizer and is given in terms of weights of basis airfoil shapes. Therefore the parameters of interest here are the basis shape weights, because the system level optimizer needs gradients with respect to these variables. The basis function weights for this problem, P_1, P_2, P_3 correspond to the airfoils E-387, NACA 64A010, and the S2055 respectively. The starting values for the weights are $p_1 = 1.0$, $p_2 = 0.0$, and $p_3 = 0.0$. Therefore we are just using the E-387 as the airfoil. The other weights are perturbed to find the sensitivities in both methods.

The design variables, **x**, for the problem include three vertical displacements of the cubic spline nodal points that divide the exterior airfoil into two smaller airfoils. The vertical displacements are referenced from the camber line.

The optimization problem for this specific example is to maximize the lift generated by the separated conforming airfoils, subject to a minimum lift to drag ratio and bounds on the design variables for structural reasons. Mathematically this is written as,

$$\begin{aligned} &\underset{\mathbf{x}}{\text{minimize :}} \quad F = -c_l|_{split} \\ &\text{subject to :} \\ &\begin{pmatrix} 20 \\ -0.0267 \\ -0.0299 \\ -0.0148 \end{pmatrix} \leq \begin{pmatrix} c_l/c_d \\ x_1 \\ x_2 \\ x_3 \end{pmatrix} \leq \begin{pmatrix} \infty \\ 0.0267 \\ 0.0299 \\ 0.0148 \end{pmatrix}. \end{aligned}$$

The angle of attack is held at a constant $\alpha = 3^o$ to decrease the computational cost of each optimization run. The airfoils were separated by a fixed value of 50% of the chord. The starting point for each design point was 0.

The Reynolds number was one and a half million, the Mach number was 0.35. An unstructured grid was used that consisted of about 60,000 elements which extended to 30 times the chord in each direction. The wall spacing on the airfoil surfaces was 0.0001. The grid around the airfoils can be seen in Figure 6 for the starting cut. The turbulence was modelled with the k-ω model.

The FUN2D (Fully Unstructured Navier-Stokes in 2D) code was used for the CFD analysis. The code was developed by NASA at the Langley Research Center[1,3]. The CFD code was run for each analysis until the RMS residue for an iteration was less than 1×10^{-11}. The convergence history for both the RMS residue and the lift coefficient for the initial design point are shown in Figures 7 and 8 respectively. These plots show that the lift coefficient has indeed reached it's steady state value. For comparison purposes the lift coefficient for the fused E-387 airfoil was 0.74708 and for the starting split configuration the lift coefficient was 1.1187.

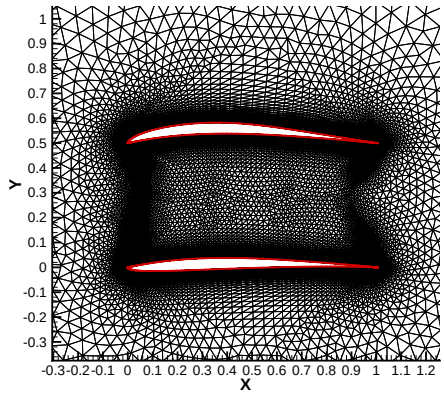

Figure 6. Unstructured mesh around the separated airfoils.

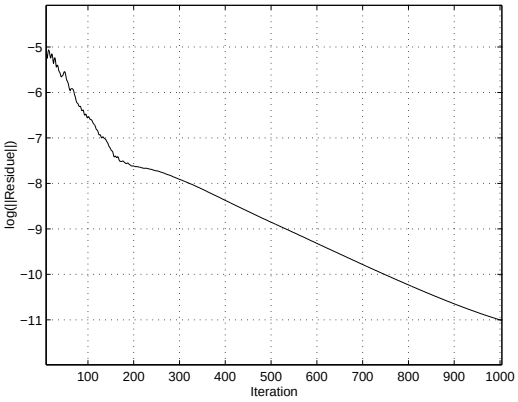

Figure 7. RMS residue convergence

The optimization was performed using MATLAB's optimization toolbox's fmincon, as was the two other example problems. The optimizer uses a Sequential Quadratic Programming (SQP) method. In this method, a Quadratic Programming (QP) subproblem is solved at each iteration. An estimate of the Hessian of the Lagrangian is updated at each iteration using the BFGS

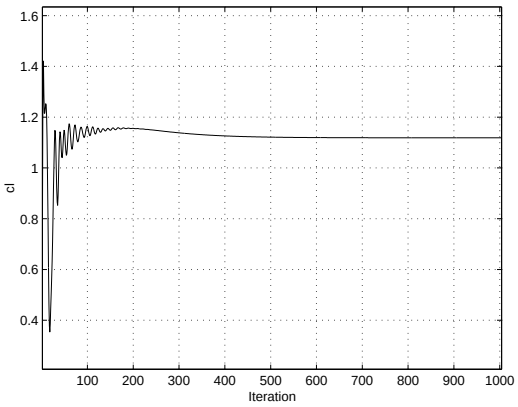

Figure 8. Lift coefficient convergence

Table 5. Conforming Airfoil Problem: Finite Difference Results

	run1	ΔP_1	ΔP_2	ΔP_3
F^*	-1.19156	-1.19859	-1.19286	-1.19458
x_1^*	0.02026	0.01595	0.01876	0.02479
x_2^*	0.02986	0.03016	0.03020	0.03013
x_3^*	0.01477	0.01492	0.01497	0.01495
CPU	2.33E4	5.50E4	3.61E4	1.63E4

formula[22].

5.3.1 Conforming Airfoil Sensitivity to External Shape Results

For the finite difference scheme the full optimization was run 4 times. One run was with no perturbation in the parameters and the other three runs each parameter was successively perturbed by a value of $\Delta P = 0.01$. The results are shown in Table 5, where run1 is the optimization with no perturbation and the ΔP_i columns are the results when the ith parameter was changed. Also the computational time in seconds are given for each run. The objective function values are the negative of the lift coefficient because of the transformation from a maximization to a minimization problem.

The total time to make the required analysis for finite differencing was 36.3 hours. The resulting sensitivities of the optimal objective function with respect to the exterior geometry parameters are,

Table 6. Conforming Airfoil Problem: Post-Optimality Sensitivity Results

	run1	ΔP_1	ΔP_2	ΔP_3
F^*	-1.19156	-1.19730	-1.19156	-1.19489
x_1^*	0.02026	0.02026	0.02026	0.02026
x_2^*	0.02986	0.02986	0.02986	0.02986
x_3^*	0.01477	0.01477	0.01477	0.01477
g_2^*	0.00000	-0.00030	-0.00035	-0.00027
g_3^*	0.00000	-0.00015	-0.00020	-0.00018
λ_2^*	0.77649	-	-	-
λ_3^*	2.95550	-	-	-
CPU	2.33E4	1.76E3	1.78E3	1.68E3

$$\frac{\mathrm{d}F^*}{\mathrm{d}P_i} \approx \begin{pmatrix} -0.7022 \\ -0.1298 \\ -0.3019 \end{pmatrix}. \tag{12}$$

For the post optimality scheme the full optimization was run only once. Then using the optimal design variable values one system analysis was performed while each of the three parameters were perturbed by the same increment as before. The resulting values are shown in Table 6, where run1 is the optimization with no perturbation and the ΔP_i columns are the results when the ith parameter is changed. The constraint values for the upper bounds on x_2 and x_3 are given as g_2 and g_3 along with there corresponding Lagrange multipliers λ_2 and λ_3. These values are given because they are the only constraints that have non-negative multipliers. The computational time in seconds are again given for each run.

The total time to make the required analysis for the post optimality method was 7.93 hours. This is a significant savings over the previous method. The resulting sensitivities of the optimal objective function with respect to the exterior geometry parameters are,

$$\frac{\mathrm{d}F^*}{\mathrm{d}P_i} \approx \begin{pmatrix} -0.6403 \\ -0.0871 \\ -0.40725 \end{pmatrix}. \tag{13}$$

The sensitivities found range from a 9% to a 35% difference from that of the finite differencing method. Since neither method gives the exact sensitivity we can not say which is better just that they are within a certain range of one another. The differences here in the sensitivities are significant but in view of the time savings the post optimality method clearly has an advantage.

Mach contours around the optimal shape can be seen in Figure 10 and the resulting pressure distribution about both the upper and lower airfoils is shown in Figure 9.

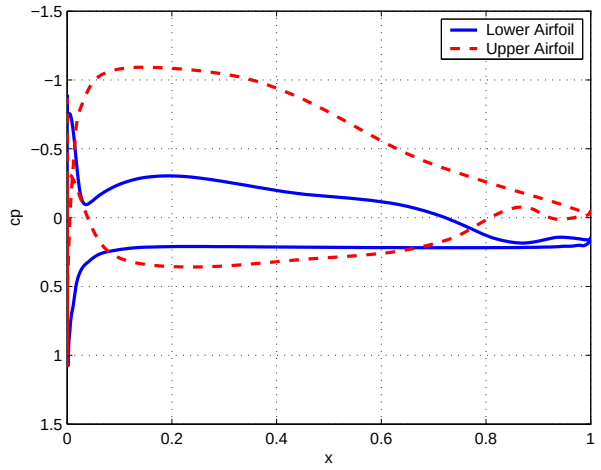

Figure 9. Pressure distribution along both airfoil surfaces of optimal design.

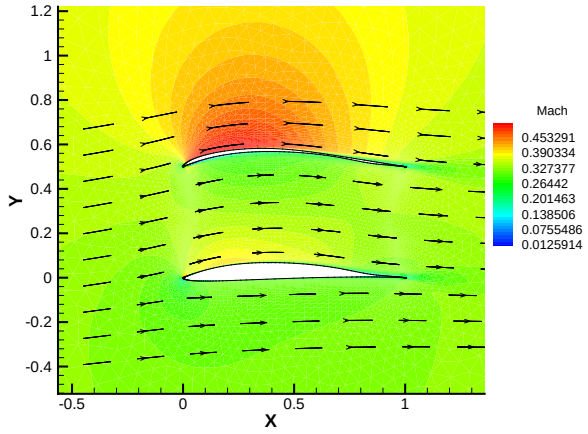

Figure 10. Mach contours and stream lines around optimal design.

6 Conclusions and Future Work

In the conforming airfoil problem the sensitivities from finite difference and post optimality methods were found to be somewhat different however both had the same sign and were within 35%. This difference was also seen in work by Sobieszczanski-Sobieski[21] et. al., in fact they found even worse agreement. Computational time however, set the two methods apart. The post optimality method took less than a fourth of the time that was needed in order to compute the same sensitivities using finite differencing. Therefore based on these results and similar findings in the simple examples the post optimality approach is much better especially when it will be used as a suboptimization problem and will have to be run several times to complete the full Buckle-wing problem.

Future work on this topic would be to change the parameter perturbation values to see how the difference between the two methods changes. Then to apply the post optimality method into the full Buckle-wing problem.

Acknowledgments

This research effort is supported in part by the following grants and contracts: ONR Grant N00014-02-1-0786 and NSF Grant DMI-0114975.

References

1. Anderson, W.K., Bonhaus, D.L.: *An Implicit Upwind Algorithm for Computing Turbulent Flows on Unstructured Grids*, Computers and Fluids, Vol. 23, No. 1. pp. 1-21, 1994.
2. Anderson, W.K., Bonhaus, D.L., *Navier-Stokes Computations and Experimental Comparisons for Multielement Airfoil Configurations*, Journal of Aircraft, Vol. 32, No. 6, pp. 1246-1253, Nov. 1995.
3. Anderson, W.K., Rausch, R.D., Bonhaus, D.L.: *Implicit/Multigrid Algorithms for Incompressible Turbulent Flows on Unstructured Grids*, AIAA 95-1740, J. Comp. Phys. Vol. 128, 1996, pp. 391-408.
4. Barthelemy, J.M., Sobieszczanski-Sobieski, J., *On Optimum Sensitivity Derivatives of Objective Functions in Non-Linear Programming*, AIAA Journal, Vol. 21, June 1983, p. 913.
5. Forster, E., Livne, E., *Integrated Structure/Actuation*

Synthesis of Strain Actuated Devices for Shape Control, Proceedings of the 42st AIAA/ASME/ASCE/AHS/ASC Structures, Structural Dynamics, and Materials Conference, AIAA 2001-1621, Seattle, WA, April 16-19.

6. Gano, S.E., Renaud, J.E., Batill, S.M., Tovar, A.: *Shape Optimization For Conforming Airfoils*, 44th AIAA/ASME/ASCE/AHS Structures, Structural Dynamics, and Materials Conference, AIAA-2003-1579, April 7-8, 2003.

7. Huyse, L., Padula, S.L., Lewis, R. M., Li, W.: *A probabilistic approach to free-form airfoil shape optimization under uncertainty.* AIAA Journal, Vol. 40, No. 9, September 2002, pp. 1764-1772.

8. McGowan, A.R., Horta, L.G., Harrison, J.S., Raney, D.L.: *Research Activities Within NASA's Morphing Program*, NATO-RTO Workshop on Structural Aspects of Flexible Aircraft Control, Ottawa, Canada, October 18-21, 1999.

9. Miley, S.J.: *A Catalog of Low Reynolds Number Airfoil Data For Wind Turine Applications*, February 1982.

10. Munk, M.M.: *General Biplane Theory*, National Advisory Committee for Aeronautics Report No. 151, 1923.

11. Nemec, M., Zingg, D.W., Pulliam, T.H.: *Multi-Point and Multi-Objective Aerodynamic Shape Optimization*, Proceedings of the 9th AIAA/ISSMO Symposium on Multidisciplinary Analysis and Optimization, AIAA 2002-5548, Sept. 4-6, 2002.

12. Norton, F.H.: *The Effect of Staggering A Biplane*, National Advisory Committee for Aeronautics Report No. 70, 1921.

13. Padula, S.L., Li, W.: *Options for robust airfoil optimization under uncertainty.* Presented at Ninth AIAA/USAF/NASA/ISSMO Symposium on Multidisciplinary Analysis and Optimization, September 4-6, 2002. also AIAA 2002-5602.

14. Padula, S.L., Rogers, J.L., Raney, D.L.: *Multidisciplinary Techniques and Novel Aircraft Control Systems*, 8th AIAA/NASA/USAF/ISSMO Multidisciplinary Analysis and Optimization Symposium, Long Beach, California, AIAA 2000-4848, September 6-8, 2000, pp. 11.

15. Pérez, V. M., Renaud, J.E., Watson, L. T., 2001, *Adaptive Experimental Design for Construction of Response Surface Approximations*, Proceedings of the 42st AIAA/ASME/ASCE/AHS/ASC Structures, Structural Dynamics, and Materials Conference, AIAA 2001-1622, Seattle, WA, April 16-19.

16. Renaud, J.E.: *Using the Generalized Reduced Gradient Method to Handle Equality Constraints Directly in a Multilevel Optimization*, Master of Science Thesis, Rensselaer Polytechnic Institute, 1989.

17. Selig, M.S., Donovan, J.F., Fraser, D.B.: *Airfoils at Low Speeds*, Soartech 8 H. A. Stokely, 1989.

18. Simpson, J.O., Wise, S.A., Bryant, R.G., Cano, R.J., Gates, T.S., Hinkley, J.A., Rogowski, R.S., Whitley, K.S.: *Innovative Materials for Aircraft Morphing*, SPIE'S 5th Annual International Symposium on Smart Structures and Materials, San Diego, CA, March 1-5, 1998, pp. 10.

19. Sobieszczanski-Sobieski, J.: *Sensitivity of Complex, Internally Coupled Systems*, AIAA Journal, Vol. 28, No. 1, p. 153, January 1990.

20. Sobieszczanski-Sobieski, J., Barthelemy, J.M., Riley, K.M., *Sensitivity of Optimum Solutions to Problem Parameters*, AIAA Journal, Vol. 20, Sept. 1982, p. 1291.

21. Sobieszczanski-Sobieski, J., Bloebaum, C.L., Hajela, P.: *Sensitivity of Control-Augmented Structure Obtained by a System Decomposition Method*, AIAA Journal, Vol. 29, No. 2, p. 264, 1991.

22. The Mathworks Inc.: *Optimization Toolbox User's Guide Version 2.1*, 2002.

23. Vanderplaats, G.N.: *Numerical Optimization Techniques for Engineering Design*, 3rd ed., 1999.

24. Vanderplaats, G.N., Hicks, R.M.: *Efficient Algorithm for Numerical Airfoil Optimization*, AIAA Journal of Aircraft, Vol. 16, No. 12, p. 842, December 1979.

25. Wlezien,R.W., Horner, G.C., McGowan, A.R., Padula, S.L., Scott, M.A., Silcox, R.J., Simpson, J.O.: *The Aircraft Morphing Program*, 39th AIAA/ASME/ASCE/AHS/ASC Structures, Structural Dynamics, and Materials Conference, Long Beach, California, AIAA 98-1927, April 20-23, 1998.